Electronic Supplementary Information

Zinc Mediated Crystalline Assembly of Gold Nanoclusters for Expedient Hydrogen Storage and Sensing

Srestha Basu[†], Anumita Paul[†] and Arun Chattopadhyay[† ‡]**

[†]Department of Chemistry, Indian Institute of Technology Guwahati,

Guwahati - 781039

[‡]Centre for nanotechnology, Indian Institute of Technology Guwahati,

Guwahati - 781039

[*]Email: arun@iitg.ernet.in; anumita@iitg.ernet.in

Experimental Section

Materials

Tetrachloro auric acid (HAuCl$_4$, Sigma Aldrich), mercaptopropionic acid (MPA, Sigma Aldrich, 99%), histidine (His, Fluka), zinc acetate dihydrate (Merck, 99%), Rhodamine 6G (Sigma, 98%), quinine sulphate (Sigma Aldrich), sulphuric acid (Merck), potassium bromide (Sigma Aldrich) were used as procured without further purification. Water of Milli-Q grade has been used for experimental purpose.

Instruments

(a) Optical Measurements. Fluorescence and UV-Visible study of as synthesized and zinc added gold nanoclusters was done using HORIBA Jobin Yvon FluoroMax-4 spectrofluorimeter and Perkin Elmer, Lambda 750 UV-visible spectrophotometer respectively.

(b) Transmission electron microscopy (TEM) and selected area electron diffraction (SAED) analysis. TEM and SAED analysis of ligand stabilized gold nanoclusters and their product on reaction with zinc acetate was done using JEOL JEM 2100, at maximum accelerating voltage of 200 kV. TEM samples were prepared by depoisiton of aqueous dispersion of the samples on carbon coated copper grids.

(c) Powder X-Ray diffraction (PXRD) study. PXRD analysis of crystalline complex of ligand stabilized gold nanoclusters with zinc ions was done using X-Ray diffractometer TTRAX III 18kW; Rigaku Corporation, Tokyo, Japan, CuKα (λ = 1.5406 Å). Samples for PXRD analysis were prepared by evaporation of water followed by subsequent dispersion of the sample in methanol or water and evaporation of methanol.

(d) Fourier transform infrared (FTIR) spectroscopy. FTIR analysis of Au$_{14}$ nanoclusters and zinc added nanoclusters was done using FTIR spectrophotometer Thermo Scientific

2

instrument. Samples for FTIR were obtained by lyophilization of the aqueous dispersions of the samples.

(e) Time resolved photoluminescence (TRPL) study. Life-Spec-II spectrofluorimeter (Edinburgh Instrument) was used to perform TRPL analysis of as synthesized gold nanoclusters and zinc added gold nanoclusters. TRPL study was performed in continuous stirring conditon to prevent settlement of the samples.

(f) Matrix assisted laser desorption ionization –time of flight (MALDI-TOF) mass spectrometry. MALDI analysis was performed using Applied Bio systems 4800 Plus MALDI TOF/TOF analyzer. Sinnapinic acid was used as the matrix for MALDI analysis.

(g) Small angle X-Ray scattering (SAXS) experiment. SAXSpace instrument, Anton Paar, X-Ray generator ID3003 - Cu Kα (α = 0.1542 nm) was used for SAXS analysis.

(h) Thermogravimetric analysis (TGA). Perkin Elmer 4000 was used to record the TGA spectrum of crystalline complex of gold nanoclusters. Samples for TGA were prepared in a manner analogous to PXRD.

(i) Gas adsorption analysis. Sorption of hydrogen gas within crystalline complex of gold nanoclusters was performed using High pressure gas sorption analyser, Quantachrome instruments isorb HP1. For hydrogen sorption analysis, synthesis of crystalline complex of gold nanoclusters was performed following protocol discussed below using methanol or water as solvent. The obtained precipitate was dried by evaporating the solvent to dryness and purified by subsequent washing with methanol.

(j) Gas chromatography. Evolution of hydrogen from the crystalline complex upon reduction of pressure was verified by gas chromatography using Agilent 7890A Network Gas Chromatograph system. The vial containing hydrogen purged dispersion of crystalline complex of gold nanoclusters was exposed to atmosphere and the solution was purged with

argon to ensure removal of dissolved gases. The vapour evolved from the dispersion was collected therein with a Hamilton syringe and the experiment was performed.

(k) Fluorimetric sensing of hydrogen adsorption and desorption: 2 mg of crystalline complex of gold nanoclusters was dispersed in 3 mL of hexane. The dispersion was purged with hydrogen using a hydrogen balloon.

(l) Computational analysis. Structural modelling of the crystalline complex was done using Avogadro software.

(m) Simulation of ESI- MS spectra: The ESI-MS spectrum of $Au_{14}MPA_7His_5$ has been simulated using mMass – mass spectrometry tool.[1-3] The simulated ESI-MS spectrum has been superimposed with the experimental spectrum in Fig. S11.

Synthetic Methods

(a) Synthesis of gold nanoclusters. 10 mM $HAuCl_4$ was added to 10 mL of water followed by addition of 0.35 mL mercaptopropionic acid (0.11 M) under constant stirring at room temperature. To the resulting solution, 30 mg of histidine was added, which resulted in the formation of yellow luminescent gold nanoclusters.

(b) Formation of crystalline gold nanoclusters. To the solution of as synthesized gold nanoclusters, 150 mg of zinc acetate was added, which resulted in gradual settlement of colourless crystalline compound. The crystalline compound thus formed was brightly luminescent upon UV irradiation at 300 nm.
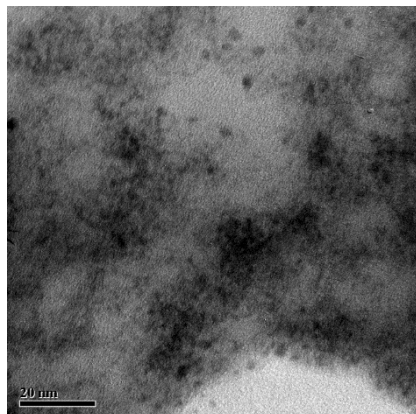
Fig. S1 Transmission electron microscopic (TEM) image of as-synthesised Au_{14} nanoclusters. The image shows formation of particles of diameter less than 2 nm, which had undergone aggregation, following evaporation of the dispersion on the TEM grid.
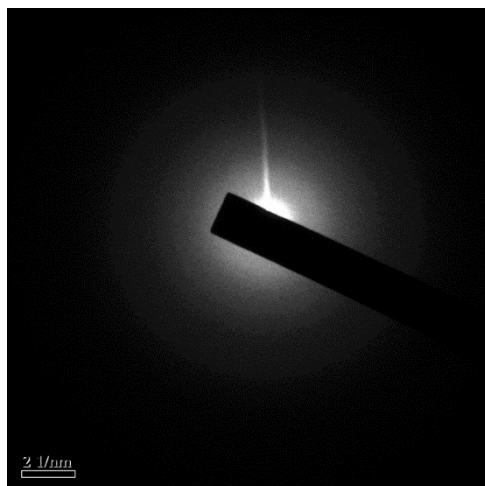
Fig. S2 Selected area electron diffraction (SAED) pattern of the sample containing the as-synthesised Au_{14} nanoclusters**.** As is evident from the image, the as-synthesized Au_{14} nanoclusters were devoid of distinct electron diffraction pattern
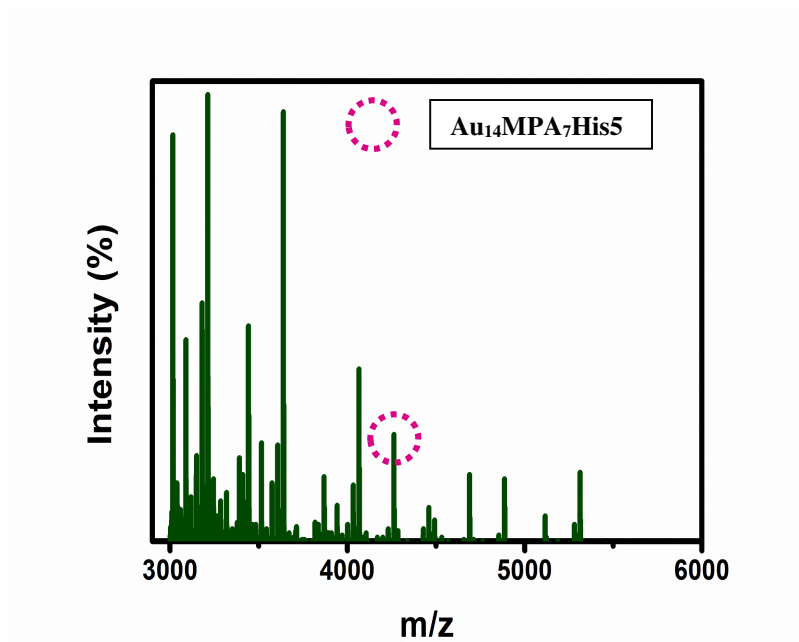
Fig. S3 Matrix assisted laser desorption ionization - time of flight (MALDI -TOF) mass spectrum of as synthesised Au_{14} nanoclusters. The spectrum was collected in reflector negative mode. The m/z value corresponding to Au nanocluster (encircled in dots) is m/z 4261, which substantiates the molecular formula of the cluster to be [$Au_{14}MPA_7His_5$].
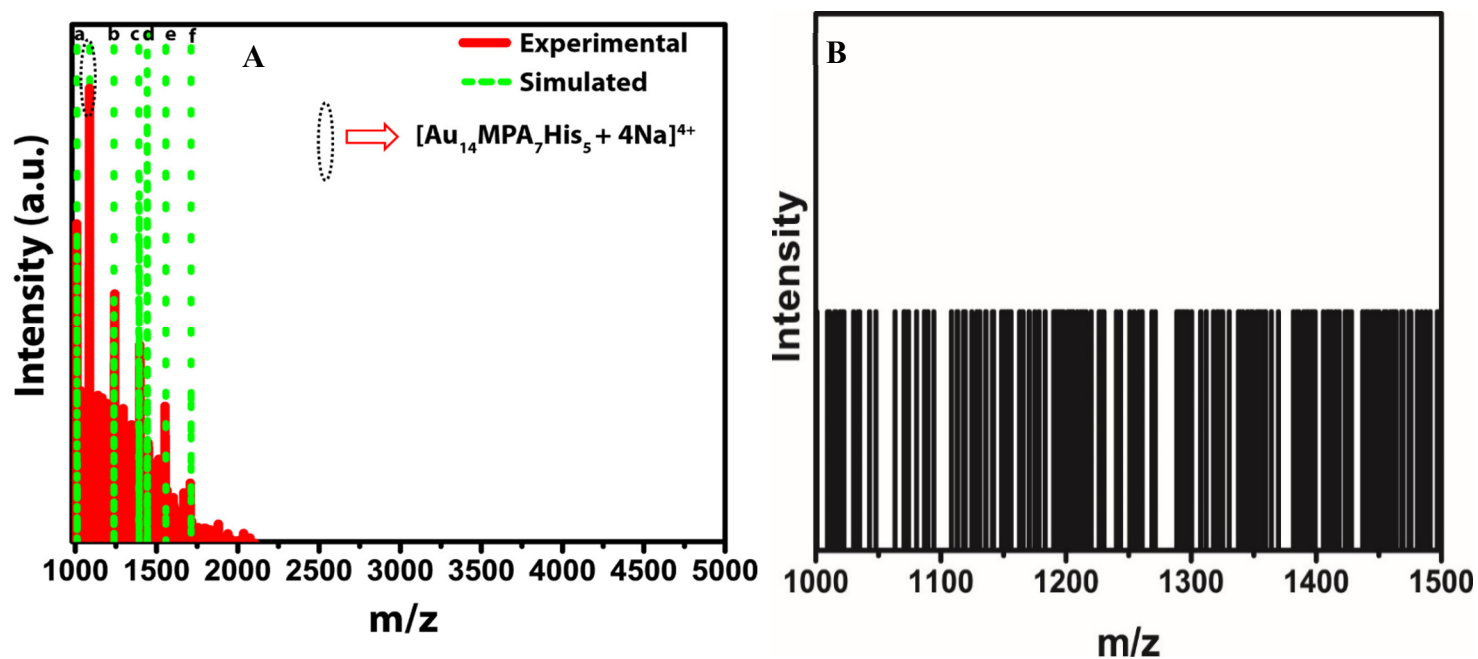
Fig. S4 Electrospray ionization mass spectra (ESI-MS) of **(A)** $Au_{14}MPA_7His_5Zn$. The fragments in addition to the parent peak (assigned in the figure legend) are as follows: a: $[Au_{14}MPA_7His_3 + 4\ Na]^{4+}$; b: $[Au_{14}MPA_7His_1 + 3\ Na]^{3+}$; c: $[Au_{14}MPA_7His_4 + 3\ Na]^{3+}$; d: $[Au_{14}His_2 + 2\ Na]^{2+}$; e: $[Au_{14}His_4 + 2\ Na]^{2+}$ and **(B)** a mixture of histidine and MPA. The simulated ESI-MS spectrum (serrated lines) has been superimposed with the experimental spectrum (solid lines).
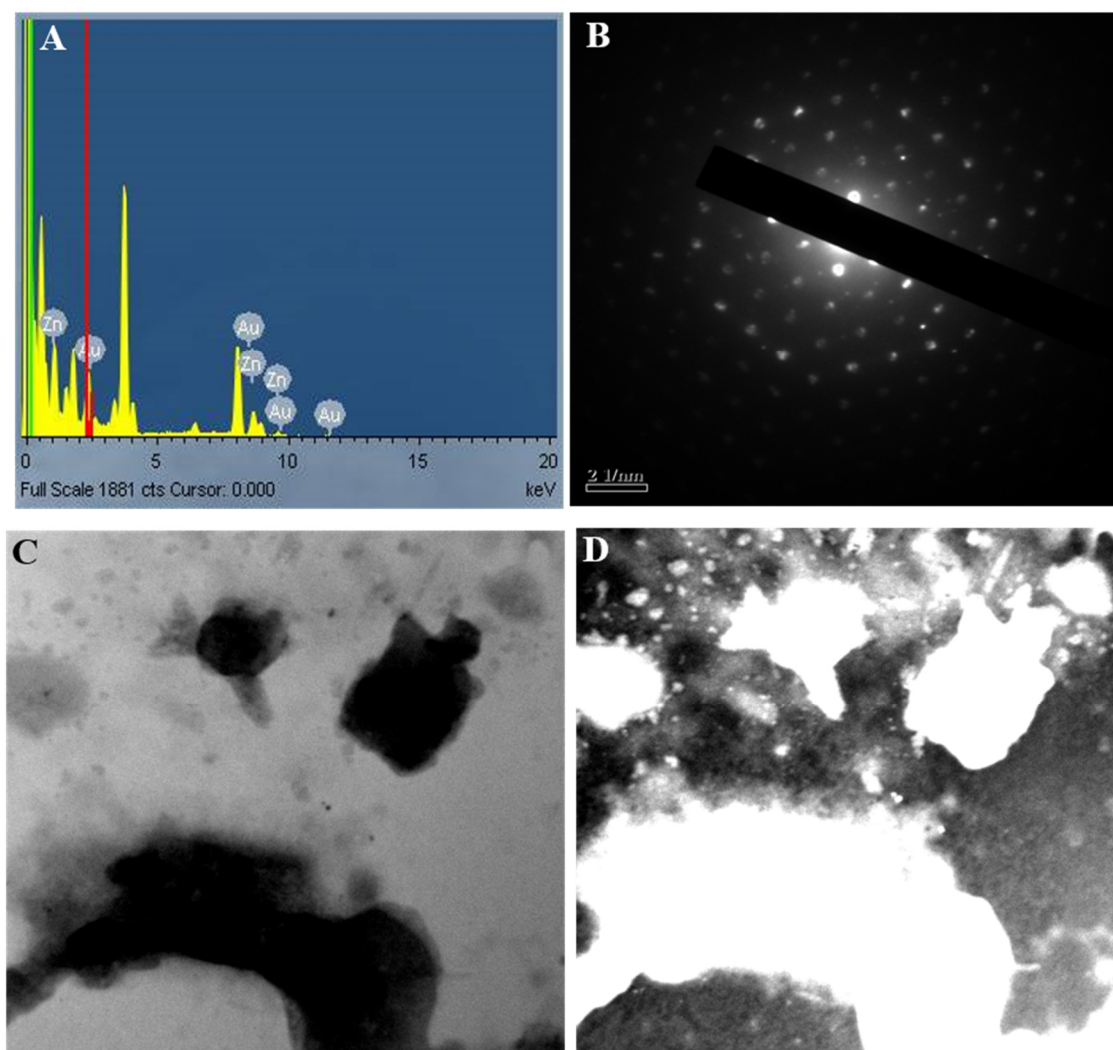
Fig. S5 (**A**) STEM-EDX analysis of $Au_{14}MPA_7His_5Zn$. (**B**) Selected area electron diffraction (SAED) of crystalline complex of $Au_{14}MPA_7His_5Zn$. (**C**) Bright field scanning transmission electron microscopic (STEM) image of $Au_{14}MPA_7His_5Zn$. (**D**) Dark field STEM image of $Au_{14}MPA_7His_5Zn$.
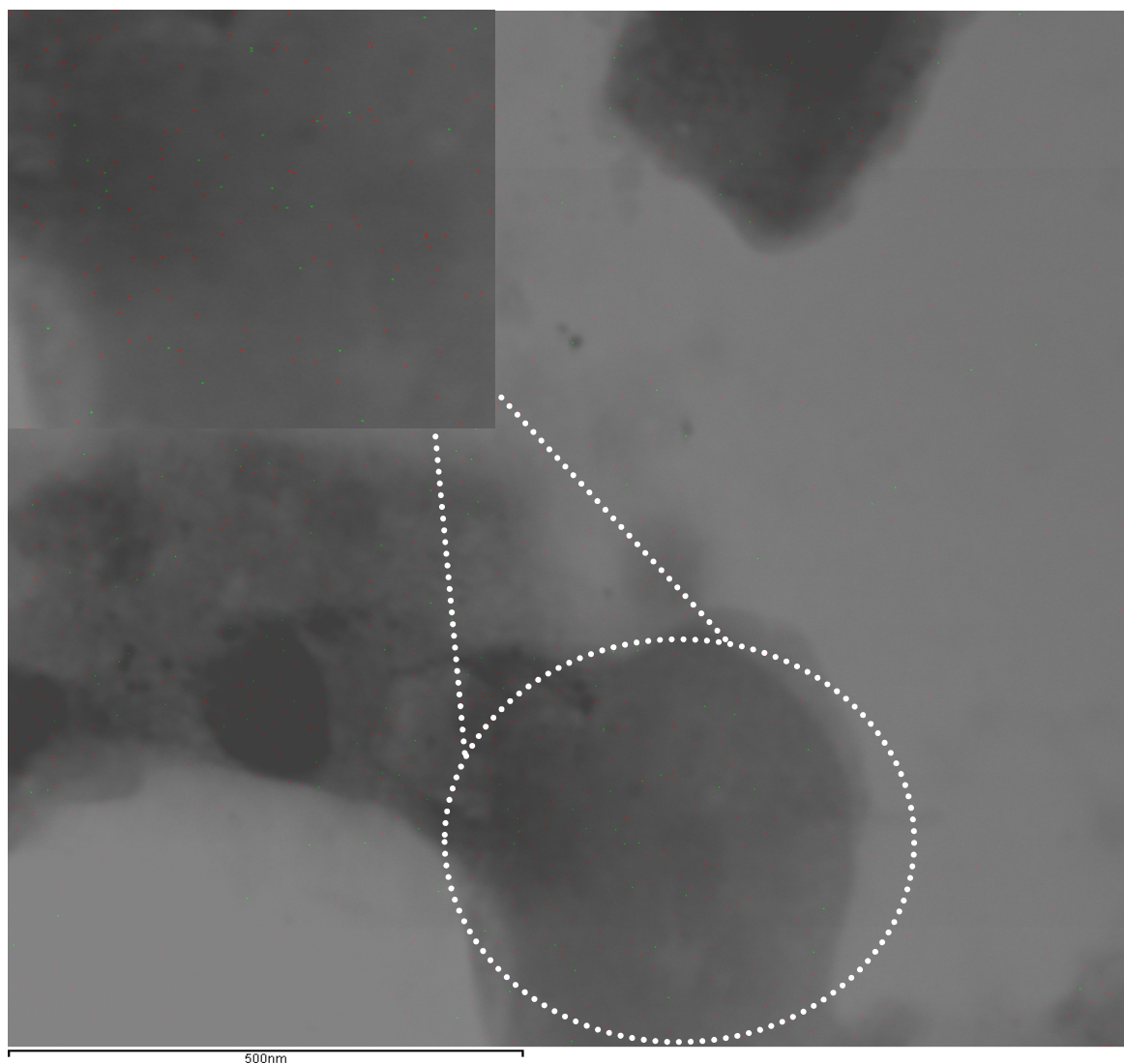
Fig. S6 Elemental mapping analysis of $Au_{14}MPA_7His_5Zn$. Au is represented by green spot and zinc by red spot.
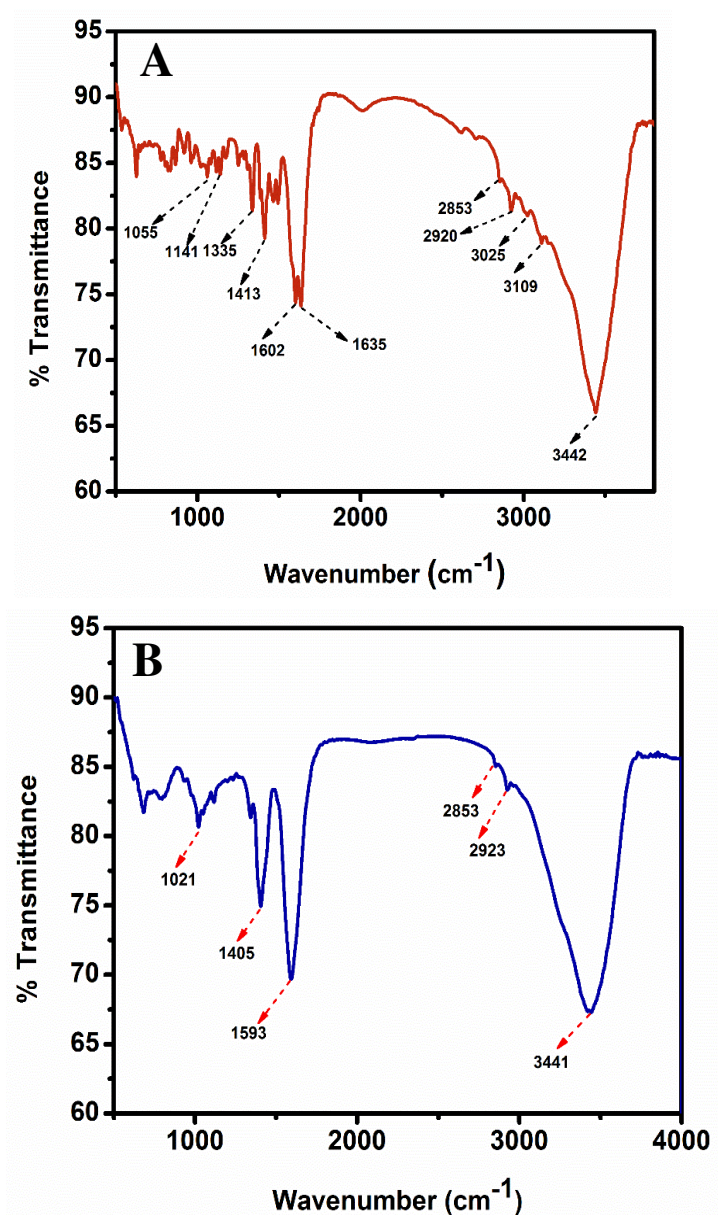
Fig. S7 FTIR spectra of (**A**) ligand-stabilized Au_{14} nanoclusters and (**B**) the product of their reaction with zinc acetate ($Au_{14}MPA_7His_5Zn$).
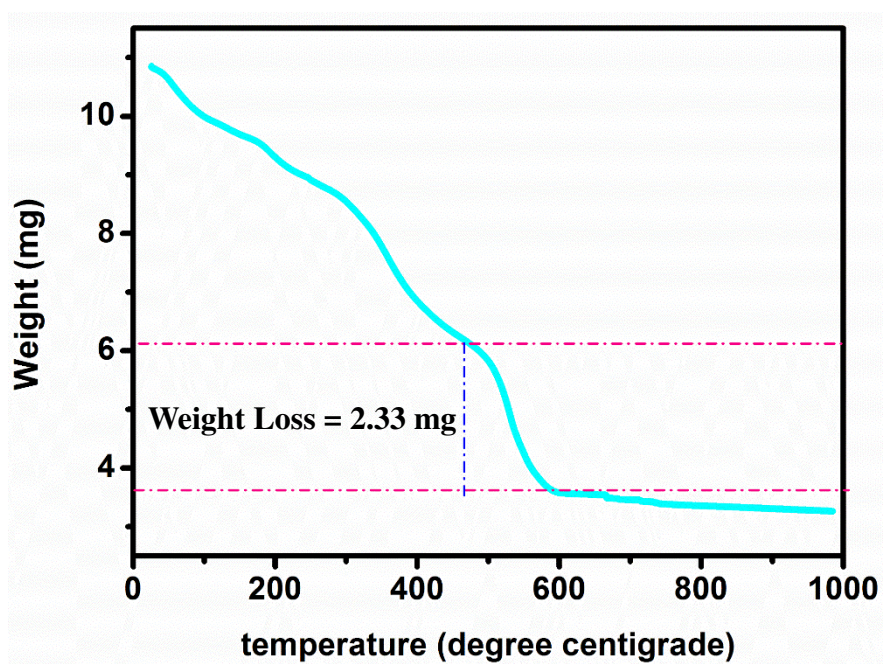
Fig. S8 Thermo-gravimetric analysis of the complex ($Au_{14}MPA_7His_5Zn$) produced from the reaction of ligand-stabilized Au_{14} nanoclusters and zinc acetate.

Fig. S9 Powder X-ray diffraction pattern of complex ($Au_{14}MPA_7His_5Zn$) produced from the reaction of ligand-stabilized Au_{14} nanoclusters and zinc acetate.

Fig. S10 Small angle X-ray scattering of the complex ($Au_{14}MPA_7His_5Zn$) produced from the reaction of ligand-stabilized Au nanoclusters and zinc acetate. Particle size distribution calculated from small angle X-ray scattering of complex ($Au_{14}MPA_7His_5Zn$) produced from reaction of ligand-stabilized Au_{14} nanoclusters and zinc acetate.

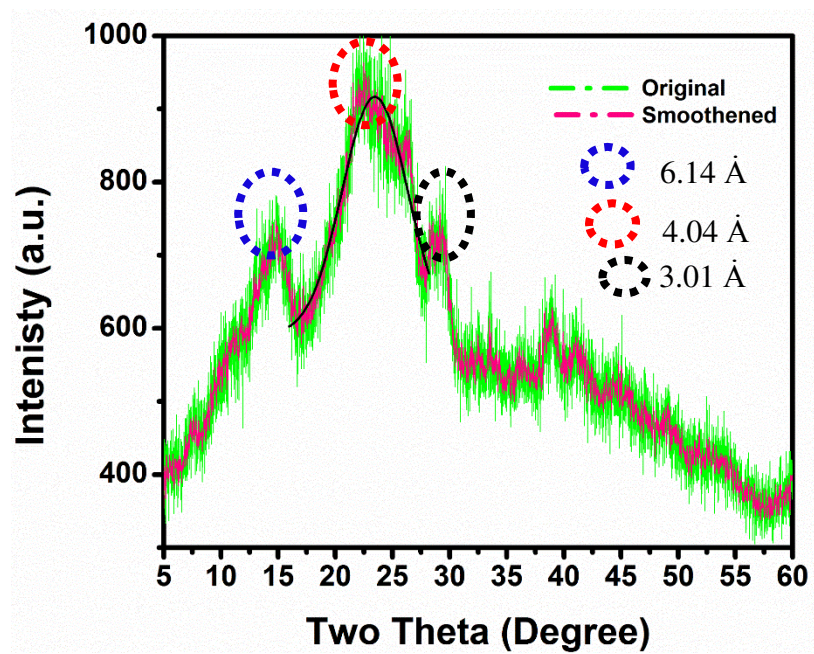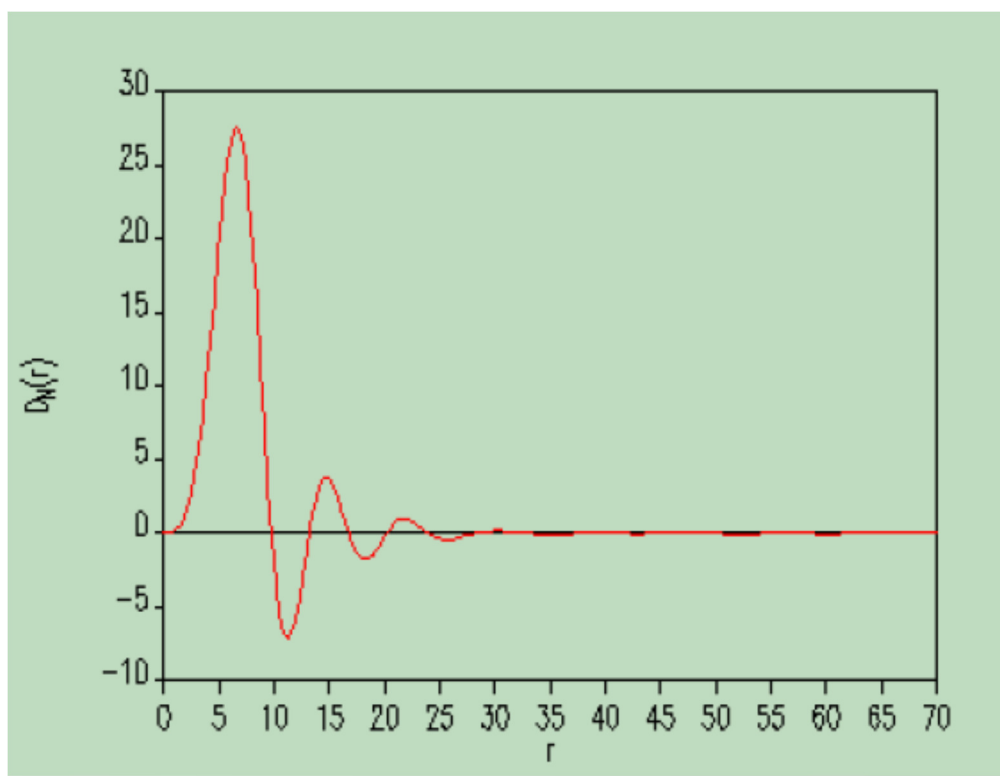**Quantum yield calculation in reference with quinine sulphate in 0.1 M H_2SO_4:**

The quantum yield of as-synthesised Au_{14} nanoclusters was calculated with respect to quinine sulphate based on the formula,

$$Q_{NCs} = Q_{Ref} \times (I_{NCs}/I_{Ref}) \times (A_{Ref}/A_{NCs}) \times (n^2{}_{NCs}/ n^2{}_{Ref})$$

Here, Q_{NCs}= Quantum yield of Au NCs;

Q_{Ref} = Quantum yield of quinine sulphate which is reported to be 0.54

I_{NCs} = Area under photoluminescence curve of Au NCs;

I_{Ref} = Area under photoluminescence curve of quinine sulphate;

A_{Ref} = Absorbance of quinine sulphate;

A_{NCs}= Absorbance of Au NCs;

n = Refractive Index of Au NCs and quinine sulphate respectively;

The concentrations of all solutions were adjusted such that the optical density values remained below 0.1. The calculated value of quantum yield of as-synthesised Au nanoclusters is reported to be 1.2 %

Table S1 Decay Parameters of ligand stabilised Au_{14} nanoclusters and the product of their reaction with zinc acetate. The analysis was performed using laser of 375 nm. The data were fitted using tri exponential fitting parameters.

Sample	A_1 (%)	r_1 (ns)	A_2 (%)	r_2 (ns)	A_3 (%)	r_3 (ns)	χ^2
Ligand stabilised Au nanoclusters	22.01	0.527	37.01	5.130	40.98	50.739	0.97
Zinc added Au nanoclusters	5.128	7.575	19.99	144.100	74.88	1263	1.08

Table S2 Surface area and pore volume of crystalline complex of gold nanoclusters. Analysis is based on adsorption of nitrogen gas.

Sample	Surface area	Pore volume
Product of reaction of ligand stabilzed gold nanoclusters with zinc acetate	2.917 m²/g	0.009 cc/g

Discussion

A. Details of synthesis of gold nanoclusters

(a.)   The synthesis of Au_{14} nanoclusters involved sequential addition of 3-mercaptopropionic acid (MPA) and histidine to $HAuCl_4$. In the first step, Au precursor ($HAuCl_4$) was added with MPA. This led to the formation of Au (I)-thiolate complex as indicated by immediate discharge of greenish yellow color of $HAuCl_4$ on addition of MPA, resulting into a white colored solution. The formation of such Au (I) thiolate complexes is justified by previous reports.[4] Thus obtained solution was further added with histidine, which can be considered to have reduced Au (I) to Au (0), resulting in the formation of Au_{14} nanoclusters. The reduction of Au salt to Au (0) by histidine has also been reported.[5]

(b.) Explanation of charge balance of the synthesised crystalline complex

Molecular formula: $Au_{14}MPA_7His_5Zn$

pH prior to crystallization: > 7.59

At pH greater than 7.59, histidine exists as neutral molecule;

So zinc binds to double bonded nitrogen via coordinate bond.

After crystallization, the pH drops to 6. Also, the pK_a of side chain of histidine is 6, which leads to protonation of side chain.

Thus at this stage, there are 5 positive charges owing to the presence of 5 histidine. Another +2 charges are there due to zinc. Thus total positive charge is 7. That is +7.

Now, pka of carboxylate group of mercaptopropionic acid is 4.3.

Thus at pH above 4.3, MPA will exist as carboxylate. That is negatively charged. There are seven such negative charges as there are seven MPAs.

18

These seven negative charges exactly balance the seven positive charges, thereby making the crystal neutral. This calculation also substantiates the presence of seven MPA and five histidine moieties as obtained from MALDI-TOF analysis.

B. Structural analysis

(a) FTIR:

FTIR spectroscopic analysis revealed that the binding of zinc ion to His might have been through imidazole nitrogen. This is based on the observation that the characteristic peak due to C-N stretching at 1635 cm^{-1} - although present in ligand-stabilized Au_{14} nanoclusters (Fig. S7A) - was absent in $Au_{14}MPA_7His_5Zn$ (Fig. S7B). The stretching frequency (C=C) due to the aromatic ring at 1602 cm^{-1} in the Au nanoclusters was shifted to 1593 cm^{-1} in the case of the complex, possibly due to complexation of the zinc ion with C=N of the same ring. Interestingly, the stretching frequencies corresponding to alkane C-H at 2920 cm^{-1} and 2853 cm^{-1} for ligand stabilized Au_{14} nanoclusters remained nearly unaltered even after complexation. The said observations clearly indicated that the complexation of zinc with His occurred through the imine nitrogen.

(b) TGA:

Thermo-gravimetric analysis (TGA) of the complex (Fig. S8) revealed no significant weight loss up to 250 °C. The total content of histidine in the mixture of MPA-His is 50.33% (as evident from MALDI-MS analysis). The decomposition temperature of histidine is reported to be 282 °C. As per the TGA graph (Fig. S8), a continuous weight loss occurs from 280 °C (initiated at 264 °C). This loss in mass is assigned to the loss of histidine from the composite mixture of MPA-His. As is evident from the TGA graph, the weight loss is about 55% of the

total weight loss (barring the weight loss due to ZnHis$_5$MPA$_7$). This weight loss, thus, is in close agreement with the composition of histidine in the composite mixture of MPA-His determined from MALDI –TOF analysis. On the other hand, a significant weight loss (about 38.5 % of the weight present at 480 °C) occurred at a temperature of 529 °C. This may be attributed to loss of ZnHis$_5$MPA$_7$, which constitutes 36.2 % of the total weight of $Au_{14}MPA_7His_5Zn$. Also, 61.5 % of the amount of sample remained nearly intact up to a temperature of 1000 °C. This mass percentage is in concordance with the mass of Au_{14} out of total mass of $Au_{14}MPA_7His_5Zn$ that is 63 %.
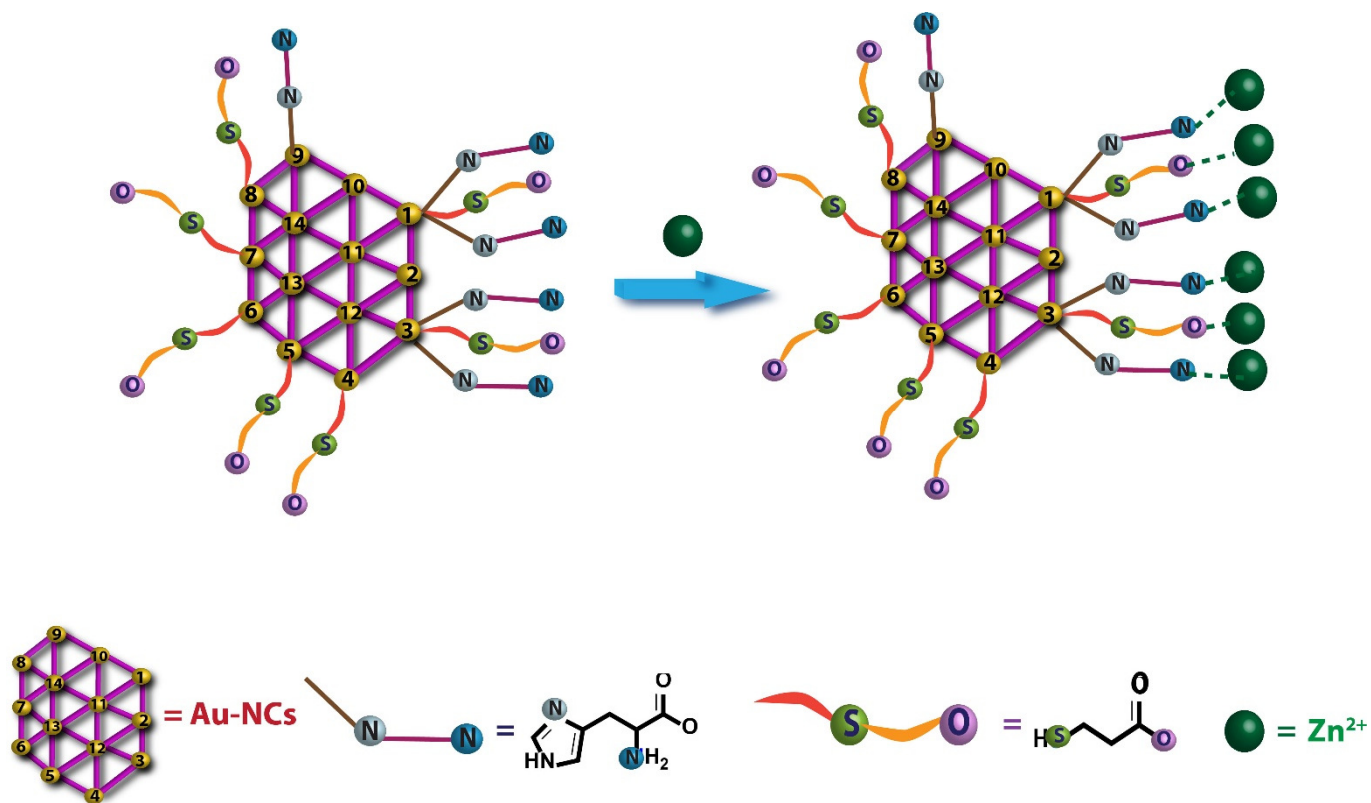
(c) Computational analysis:

The structure of the crystalline complex, as obtained from the electron diffraction and other analyses, was further substantiated by computational modelling using Avogadro. Briefly, in the energy optimized structure (Fig. 3A), the Au_{14} clusters were considered planar with five peripheral Au atoms bonded to five MPA (each MPA being coordinated to a single Au atom). In addition, two peripheral Au atoms were bonded to four His ligands and two MPA ligands (i.e. two His ligands and one MPA ligand being coordinated to each Au atom). One peripheral Au atom was bonded to one His ligand, while two Au atoms remained non-coordinated. Coordination of MPA to constituent Au of gold nanoclusters was likely to be through sulphur atom, owing to the aurophilicity of the latter. Likewise, His was considered to stabilize the clusters through nitrogen atom of the main chain amino group, while nitrogen atom of the side chain imidazole group was involved in ligating the zinc ion. The peripheral Au atom of the nanoclusters constituting the hexagonal unit cell of the crystal structure was bonded to two histidine and one MPA ligands (marked as Au1 and Au3 in Fig. 3B and as in the schematic shown below). Each zinc ion was ligated to one of the two His ligands being coordinated to single Au atom and likewise with a His ligand and MPA ligand of other two Au atoms of two

different clusters to afford the formation of two connected hexagons, ultimately leading to tri-coordination of both zinc ion and gold atom in the plane.

Interestingly, the distance between zinc ions and nearest (peripheral) Au atom in a trigonal geometry was calculated to be 6.7 Å. This is consistent with the observed electron diffraction pattern (Table S3). As a matter of fact, the constituent atoms of Au clusters and zinc ions were positioned in alternate vertices of connected hexagons (in two dimensions) with distances between zinc and a peripheral Au atom in closest proximity, corroborating the electron diffraction data. However, while coordination of zinc ion to three Au atoms (each being a part of individual Au_{14} clusters) defines a trigonal plane (with bond distance of 6.7 Å), extension of crystal structure through the axial dimension was achieved via Au-Au (marked as Au1 and Au3) moiety of Au_{14} clusters, with His and MPA ligated Au atoms connecting two layers of hexagon and a non-ligated Au atom in between. In this dimension, the interlayer distance of separation was theoretically computed to be 5.0 Å, which is in good agreement with the experimentally obtained value of 4.8 Å (Fig. 2C) from SAED pattern and 5.0 Å from HRTEM analysis (Fig. 2D). Substantial degree of concordance between theoretically computed value and experimentally observed value was achieved (Table S4). Moreover, as the two peripheral Au atoms of Au_{14} clusters were involved in forming the edges of hexagon and interconnecting two such layers, the remaining constituents of clusters were positioned perpendicular to the hexagon. One such Au constituent of the clusters (marked 8 in Fig. 3B), at a distance of 6.7 Å from the Au atom defining the edge of each hexagon (marked 1 in Fig. 3B) was situated at the center of the hexagon. This is apparent from SAED pattern (Fig. 2B) which shows that each hexagon possesses a center corresponding to the distance from the edge being equivalent to 6.7 Å. Thus, the distance of 6.7 Å obtained from theoretical optimization matched closely with that of the distance of center to edge of a hexagon in diffraction pattern, thereby justifying the positioning of Au atom of cluster at the center of hexagon in theoretical

model (Fig. 3B). Also, as observed from SAED, diffraction spots at every separation of 0.45 Å^{-1} (in reciprocal space, and corresponding to 2.3 Å in real space) are brighter in intensity. The enhanced brightness of such group of spots over others could be explained by the proposition that separation of 0.45 Å^{-1} corresponding to Au – Au distance of 2.5 Å in computationally optimized structure, superimposed with that due to Au – Zn distance of 6.7 Å at an interval of two diffraction spots. Besides, as mentioned above, the Au atom forming the edge of hexagon was coordinated to two His ligands and one MPA ligand. In this regard, the distance between Au and sulphur atom (of MPA) was theoretically calculated to be 2.3 Å; in addition, Au-nitrogen (of His) distance was computed to be 2.0 Å. Thus, diffraction due to Au- sulphur as well as Au – nitrogen appeared symmetrically at every 0.45 Å^{-1} (in reciprocal space and 2.2 Å when converted to distance in real space), along the six-fold axes in the plane constituting the hexagons. This also leads to appearance of diffraction spots with increased intensity at an interval of two diffraction spots with comparatively lower intensity. The corroboration of the experimentally observed distances with that of computationally obtained distances along with the error percentages have been tabulated in Tables S3 and S4. Additionally, the clusters interlinked the hexagonal layers in alternate fashion thereby maintaining the symmetry of the structure. In other words, the two hexagonal planes are connected by Au_{14} clusters –which themselves are in a plane perpendicular to the hexagonal planes – and as shown in Fig. 3B

Scheme S1. Schematic representation of complexation reaction between ligand stabilized (MPA and His) gold nanoclusters and zinc ions. Each zinc ion in the complex is a part of a hexagon.

(d) PXRD and SAXS analysis:

A fair degree of accordance was observed between the inter-planar dimensions obtained from SAED analysis and powder X-ray diffraction pattern (Fig. S9, ESI). While the peak at a value of $2\theta = 22°$ yielded a lattice spacing value of 4.0 Å, the peak at $2\theta = 14.4°$ provided a d-spacing value of 6.1 Å. This is in fair agreement with the lattice spacing values of 4.8 Å and 6.7 Å as obtained from SAED analysis. Further, the existence of planes with interplanar separation of 2.2 Å, as revealed from SAED is justified by the peak in XRD at two theta value of 29.6° corresponding to d-spacing of 3.0 Å (Table S3 and S4). Even more intriguingly, the particle size of 5.2 nm, as calculated by employing Scherrer equation to the peak at 22°, was in agreement with that obtained from small angle X-ray scattering (SAXS) analysis (5.5 nm) (Fig. S10, ESI).

(e) Assignment of the parent peak in the ESI-MS:

PK_a of carboxylate of MPA = 4.3

PK_a of carboxylate of Histidine = 1.8

pH of cluster is > 7 (before crystallization)

If we assume the formula of the compound to be $[Au_{14}MPA_7His_5]$, then at pH > 7, there will be 12 negative charges i.e., carboxylic acid groups (7 of MPA and 5 of histidine) will exist as carboxylate ions. The imidazole nitrogen remains positively charged (so 5 positive charges)

At the ionization (positive) chamber,

12 protons neutralizes the 12 negative charges of carboxylate groups.

In this condition, the molecule is otherwise neutral but 5 nitrogen of 5 histidine remains protonated.

Assuming one out of 5 such nitrogen being deprotonated in the equilibrium, now 4 protonated nitrogen remains

Hence, the total mass of the compound now becomes [4261+7 (protons from protonated carboxylate of MPA) + 5 (protons from protonated carboxylate of histidine) + 4 (protons from protonated nitrogen of histidine) – 3 (3 protons of carboxylic acid replaced by 3 sodium ions) + (23*3) (replacing sodium ions)] = 4343

Total mass is 4343

Now the total charge is -12 + 16 = +4

Thus m/z = 4343/4 = 1085.75 ~ 1086 (parent peak)

C. Calculation of complexation constant:

Having established the structure of the complex from theoretical and experimental perspectives, it was deemed important to set up a chemical equation governing the process of complexation and quantitate the same in terms of complexation constant. This was achieved by pursuing reaction of the as-synthesized Au_{14} nanoclusters with different concentrations of Zn^{2+}. The reaction as well as formation of product was followed by the change in photoluminescence intensity for the peak at 576 nm. It was observed that for an initial concentration of 0.70 mM $HAuCl_4$, 0.69 mM of Zn-acetate was needed to reach the saturation in luminescence intensity increase, indicating completion of the reaction. Occurrence of equimolar reaction between Au nanoclusters and zinc ions, in conjunction with the structure obtained from computational analysis, forms the basis of assumption of one is to one

stoichiometric correspondence between Au nanocluster and zinc ion. The reaction between zinc ions and Au NCs can then be written as in equation (1), with an expression for complexation constant as in equation (2).

$$AuNC + Zn(2+) \rightarrow ZnAuNC \qquad (1)$$

$$K = [ZnAuNC]/[AuNC]\,[Zn(2+)] \qquad (2)$$

The concentration of the luminescent chemical species involved in equation (2) can be correlated to their emission intensities (precisely, to the area under the luminescence curve). This leads to equation (3) where,

I_O = Area under the luminescence curve solely due to Au NCs (i.e. in absence of Zn(2+))

I = Area under the luminescence curve of Au NCs in presence of Zn(2+)

[Zn(2+)] = Concentration of Zn^{2+} in the reaction system

$[Zn(2+)]_\infty$ = Concentration of Zn^{2+} when all of Au NCs is consumed.

$$Log\,\frac{I_{effective}}{I_O} = LogK + Log[Zn(2+)] \qquad (3)$$

with $I_{effective} = I - I_O - \dfrac{[Zn(2+)]\,I_O}{[Zn(2+)]_\infty}$

Thus the plot of Log [$I_{effective}$]/ [I_0] against Log [Zn^{2+}] would give a straight line from the intercept of which the value of complexation constant (K) can be evaluated. The value of complexation constant calculated from equation (2) is reported to be $(9.7 \pm 6.6) \times 10^6$ M^{-1} (Fig. 1 D and E).

D. Time resolved photoluminescence study:

The luminescence enhancement was further probed by TRPL. The study indicated large change in lifetime of Au_{14} nanoclusters upon complexation with zinc ions (Fig. 1 B and C). The

lifetime of the longest emitting component of the nanoclusters was recorded to be 50.74 ns, whereas upon complexation with zinc ions the same was observed to be 1.26 µs (Table S1). The phenomenal change in lifetime could be due to structural rigidity acquired by the nanoclusters following complexation with zinc ions. As the structure of the nanoclusters become ordered, thus rigid, upon complexation, the excited state gets stabilized – as evident from 13 nm bathochromic shift in emission maxima of nanoclusters on reaction with zinc ions. This in turn restricts the non-radiative decay, which causes enhancement in quantum yield of the clusters in the complex, thereby increasing the lifetime of the emitting species as well. Another plausible reason for enhancement in lifetime of the nanoclusters could be that due to complexation with zinc ions, the nanoclusters now are positioned in much closer proximity. This enables facile excited energy transfer within the nanoclusters, which renders increase in luminescence lifetime. The marked difference in the luminescence lifetimes of the nanoclusters prior to and following complexation with zinc ions not only substantiates the association of gold nanoclusters but also establishes the crystalline complex as a superior luminescent species when compared to as-synthesized gold nanoclusters.

E. Estimation of hydrogen release at 1.03 bar pressure:

75 mg of crystalline compound was placed in a conical flask (65 mL). The opening of the conical flask was covered with parafilm and a balloon containing hydrogen was inserted into the flask using a syringe needle. The pressure thus was approximately 1 atmosphere. After 1 h, the conical flask was deaerated by purging nitrogen for 5 min and the opening of the flask was sealed again. After 5 min, the gas within the flask was collected by a syringe. The collected gas was injected into the gas chromatograph. A sharp signal due to hydrogen was obtained. The amount of hydrogen gas was quantified in terms of volume percent normalized to the standard hydrogen gas using the gas chromatograph.

Volume % of hydrogen obtained = 0.101%

Volume of conical flask = 65 mL

Thus volume of hydrogen gas injected = 0.065 mL

Assuming ideal behavior of hydrogen gas and employing ideal gas equation to find the number

of moles of hydrogen gas injected = 0.0026866 mmol

Amount of crystalline complex subjected to hydrogen adsorption = 75 mg

Thus, amount of hydrogen gas evolved per gram of complex = 0.035 mmol/g

From the adsorption-desorption isotherm, the amount of hydrogen gas released at 1 atmosphere

pressure (i.e 1.013 bar) = 0.054 mmol/g
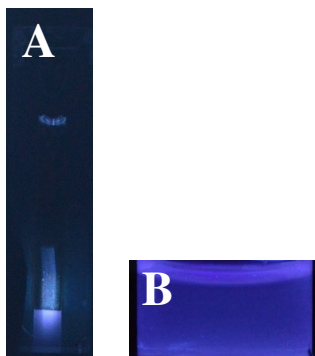
Additional Figures and Tables

Fig. S11 Digital photograph of solutions containing a mixture of MPA, His and zinc salt (control) which was non luminescent under UV irradiation i.e. excitation at 310 nm and 300 nm (**A** and **B**), respectively. The beam of the spectrofluorimeter was used as the excitation source in (**A**) while A trans-illuminator was used as the excitation source in (**B**). As the photographs depict the non-luminescence nature of the mixture in absence of $HAuCl_4$, it can be concluded that the yellow luminescence (in the presence of $HAuCl_4$) as reported in the manuscript was due to the formation of Au_{14} nanoclusters.
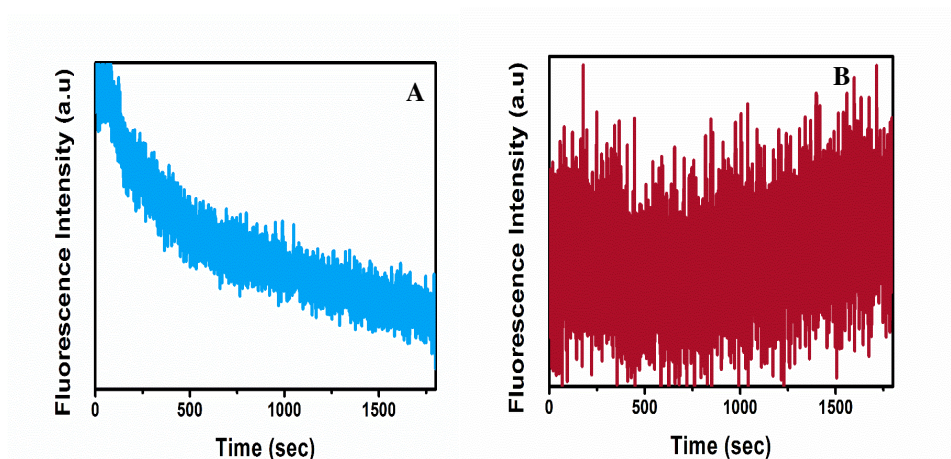
Fig. S12 Effect of photo-irradiation with time on emission intensity (excitation at 300 nm) of **(A)** rhodamine 6G dye and **(B)** as-synthesised Au_{14} nanoclusters. As is evident from the figures, rhodamine 6G underwent photo-degradation upon UV irradiation at a faster rate than Au_{14} nanoclusters.
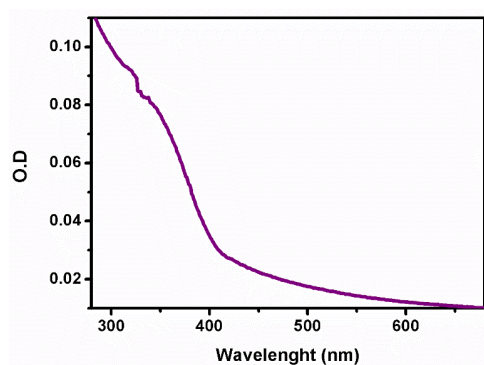
Fig. S13 UV-visible extinction spectrum of as synthesised Au_{14} nanoclusters. The figure is devoid of any significant peak in the region beyond 500 nm, suggesting that surface plasmon resonance active Au nanoparticles were not formed accompanying the synthesis of the clusters.

Table S3 Highlights of the distances between the mentioned co-ordinates (1-6 are the vertices of the first hexagon from the centre while 7-12 are the vertices of the third hexagon form the centre) of the electron diffraction pattern (Fig. 2B) and in the theoretical model (Fig. 3A) corroborating the electron diffraction pattern. *Rounded off to appropriate significant figures. The error percentage between observed and calculated distance is 3.5%. The average distance among coordinates of 7 – 12 forming a hexagon is 2.2 Å. whereas, the distances between the coordinates between Au1 – N1, N11, S1; Au2 – N2, N22, S2 and Au3- N3, N33 and S3 is 2.1 Å. The error percentage between observed and computed distance is 4.5 %.

Co - ordinates	Optimised Distances (Å)*	Co - ordinates	Observed Distances (Å)*
Au1 – Zn1	6.6	1-2	6.3
Zn1 - Au3	6.3	2-3	6.2
Au3 – Zn3	7.7	3-4	7.3
Zn3 – Au 2	6.9	4-5	6.9
Au2 – Zn2	6.5	5-6	6.8
Zn2 – Au 1	6.6	6-1	6.9
Au1 – N1	2.0	7 - 8	2.2
Au1 – N11	1.95	8 - 9	2.2
Au1 – S1	2.3	9 - 10	2.2
Au2 – S2	2.35	10 - 11	2.2
Au2 – N2	2.0	11 - 12	2.2
Au2 – N22	2.0	12 - 7	2.2
Au3 – N3	2.0		
Au3 – N33	2.0		
Au3 – S3	2.35		

Table S4 Highlights of the distances between the mentioned co-ordinates in the electron diffraction pattern (1 and 2 refers to the vertical distance between two diffraction spots) and in the theoretical model (Fig. 3A) corroborating the electron diffraction pattern. The error percentage in this dimension is 4 %.

Co - ordinates	Optimised Distances (Å)	Co - ordinates	Observed Distances (Å)
Au2 – Au22	5.0	1 - 2	4.8

Table S5 Assignment of peaks, in addition to the parent compound (4261) observed in MALDI-TOF spectra

Peak Position (m/z)	Composition
3010	$[His_{14}MPA_8]^{8-} - 8H^+$
3091	$[His_7MPA_{19}]^{8-} - 8H^+$
3148	$[His_6MPA_{21}]^{8-} - 8H^+$
3180	$[His_{13}MPA_{11}]^{-1} - 1H^+$
3211	$[His_5MPA_{23}]^{2-} - 2H^+$
3449	$[His_{10}MPA_{18}]^{9-} - 9H^+$
3637	$[His_{16}MPA_{11}]^{9-} - 9H^+$
4064	$[His_{16}MPA_{15}]^{6-} - 6H^+$

References

1. M. Strohalm, D. Kavan, P. Novák, M. Volný and V. Havlíček, *Anal. Chem.*, 2010, **82**, 4648-4651.

2. Q. Wang, M. Zhu, L. Lu, C. Yuan, S. Xing and X. Fu, *Dalton Trans.*, 2011, **40**, 12926-12934.

3. Y. Hamamoto, K. Tachibana, P. T. Holland, F. Shi, V. Beuzenberg, Y. Itoh and M. Satake, *J. Am. Chem. Soc.*, 2012, **134**, 4963-4968.

4. R. Jin, *Nanoscale*, 2010, **2**, 343-362.

5. X. Yang, M. Shi, R. Zhou, X. Chen and H. Chen, *Nanoscale*, 2011, **3**, 2596-2601.